

Calcium isotope ratios of malformed foraminifera reveal biocalcification stress preceded Oceanic Anoxic Event 2

Gabriella D. Kitch¹[✉], Andrew D. Jacobson¹, Bradley B. Sageman¹, Rodolfo Coccioni², Tia Chung-Swanson¹, Meagan E. Ankney^{1,3} & Matthew T. Hurtgen¹

Ocean acidification causes biocalcification stress. The calcium isotope composition of carbonate producers can archive such stress because calcium isotope fractionation is sensitive to precipitation rate. Here, we synthesize morphometric observations of planktic foraminifera with multi-archive calcium isotope records from Gubbio, Italy and the Western Interior Seaway spanning Cretaceous Ocean Anoxic Event 2 (~94 million years ago). Calcium isotope ratios increase ~60 thousand years prior to the event. The increase coincides with foraminiferal abnormalities and correlates with existing proxy records for carbon dioxide release during large igneous province volcanism. The results highlight Ocean Anoxic Event 2 as a geologic ocean acidification analog. Moreover, decreasing calcium isotope ratios during the event provide evidence for ocean alkalization, which could have shifted air-sea carbon dioxide partitioning. These data offer an explanation for the Plenus Cold Event and further have implications for refining ocean alkalinity enhancement, a leading anthropogenic carbon dioxide removal strategy.

¹Department of Earth and Planetary Sciences, Northwestern University, Evanston, IL, USA. ²Honorary Professor of the University of Urbino “Carlo Bo”, Urbino, Italy. ³Wisconsin State Laboratory of Hygiene, University of Wisconsin-Madison, Madison, WI, USA. ✉email: gabby.kitch@noaa.gov

Pelagic calcifiers, such as foraminifera, pteropods, and coccolithophores, compose up to 70% of the modern global marine carbonate export to the seafloor^{1,2}, and their calcification rates fundamentally link to the inorganic carbonate chemistry of seawater^{3,4}. Large and rapid increases in atmospheric CO₂ concentrations cause ocean acidification (OA), which decreases seawater pH, carbonate ion concentrations, and carbonate mineral saturation states while increasing the concentration of total dissolved inorganic carbon^{5,6}. Studies of modern planktic foraminifera impacted by OA reveal decreased biocalcification rates and other signs of stress, such as shell thinning^{7,8}. Reduced biocalcification buffers OA by increasing surface water alkalinity³, similar to other negative feedback mechanisms, such as chemical carbonate compensation and silicate weathering^{5,6}, although biological carbonate compensation is geologically instantaneous by comparison. Increased surface ocean alkalinity due to biological carbonate compensation enhances atmospheric CO₂ drawdown³, which can mitigate climate warming but further compound biocalcification stress⁶. Understanding the dynamic relationship between pelagic calcification and atmospheric CO₂ concentrations thus has key implications for quantifying the marine inorganic carbon pump and other controls on the global carbon cycle, including anthropogenic forcing⁹. It also directly underlies efforts to advance ocean alkalinity enhancement, a promising strategy for mitigating fossil fuel CO₂ emissions^{10,11} and stabilizing ocean water pH^{12,13}.

Geologic OA events provide a means to examine the biocalcification response to carbonate chemistry feedbacks during times of high background CO₂. The Cretaceous (145–66 Ma) was a hothouse period when atmospheric CO₂ may have averaged over 500 ppm (some 230 ppm higher than pre-industrial levels)¹⁴, with some intervals of significantly higher concentrations related to massive volcanic eruptions⁵. Cretaceous black shale deposits reflect short-term global carbon cycle perturbations and widespread, albeit not global, oceanic anoxia within this high-CO₂ greenhouse climate. The geologic record preserves eight oceanic anoxic events (OAEs), which are marked by organic-rich deposits, in several cases bearing large carbon isotope ($\delta^{13}\text{C}$) excursions (CIEs), as well as geochemical evidence for large igneous province (LIP) emplacement^{15,16}. For example, recent geochemical studies of the Cenomanian-Turonian OAE2 (~94 Ma), which is defined by a 3–4‰ increase in organic carbon isotope values ($\delta^{13}\text{C}_{\text{org}}$)^{17,18}, indicate that eruption of the Caribbean LIP and/or High Arctic LIP drove transient increases in atmospheric CO₂ levels¹⁹.

Several studies have implicated LIP induced-OA as the cause for faunal turnover events that occur in association with many OAEs, as well as additional morphometric changes in foraminifera and coccolithophores^{6,16,20}. Interestingly, plankton turnover events slightly precede OAEs²¹, along with size reductions of heavily calcified nannofossil taxa, such as nannoconids and schizosphaerellids²². Such is the case for OAE2, where nannofossil extinctions²² and placolith size reductions²⁰ occur just prior to the event, which is now referenced in Tethyan sections as the lower critical interval (LCI)^{23,24}. Within the LCI, foraminifera from multiple localities show evidence for reduced test size¹⁸, as well as other morphometric indicators of stress, such as reversals in coiling direction²⁵ and changes in chamber number and shape¹⁸. The detailed records of morphometric changes across OAE2 offer an excellent opportunity to evaluate the hypothesis of biocalcification stress. Test density measured by area-normalized shell weights⁷ and bulk density measured by micro-CT scanning⁸ have emerged as optimal morphometric methods for examining OA-driven biocalcification stress in modern foraminifera, but the signals are highly sensitive to dissolution and thus cannot be applied in the geologic record where

foraminifera are less pristinely preserved. Thus, to study OA-biocalcification stress in deep time, we pair existing morphometric observations with high-precision calcium isotope ($\delta^{44/40}\text{Ca}$) measurements, which offer a promising technique for constraining paleo-biocalcification.

Experiments focused on inorganic calcite precipitation show that slower precipitation rates yield smaller isotopic offsets between calcite and fluids ($\Delta\text{CaCO}_3 - \text{H}_2\text{O} = \delta^{44/40}\text{CaCO}_3 - \delta^{44/40}\text{Ca}_{\text{H}_2\text{O}}$) and thus higher $\delta^{44/40}\text{Ca}$ values compared to faster precipitation rates²⁶. Modeling studies further illustrate that rate-dependent shifts in $\Delta\text{CaCO}_3 - \text{H}_2\text{O}$ correlate with carbonate system parameters, such as carbonate ion concentration and carbonate mineral saturation states^{27,28}. Carbonate chemistry control of $\delta^{44/40}\text{Ca}$ values for some foraminifera (*Globigerinoides ruber*) has been partially demonstrated in culture (Supplementary Fig. 1), consistent with assertions that other foraminifera (*O. universa*) fractionate Ca isotopes similarly to inorganic calcite²⁹. Moreover, four geologic $\delta^{44/40}\text{Ca}$ records representing multiple candidate OA events and different marine carbonate archives, including foraminifera, mollusks, and bulk sediments, all show positive excursions consistent with reduced precipitation rates^{30–33}.

In this study, we utilize the Ca isotope proxy to comprehensively test for biocalcification stress preceding OAE2. We generated paired high-resolution and high-precision $\delta^{44/40}\text{Ca}$, $\delta^{13}\text{C}$, and $\delta^{18}\text{O}$ records for bulk carbonate and planktic foraminifera (*Rotalipora cushmani*) from the Bottaccione section in Gubbio, Italy, along with $\delta^{44/40}\text{Ca}$ and $\delta^{13}\text{C}$ records for bulk carbonate from the Aristocrat Angus (AA) core, Denver Basin, Colorado, USA (Supplementary Fig. 4). All records reveal that $\delta^{44/40}\text{Ca}$ values increased prior to the onset of the positive CIE that marks OAE2. Moreover, the pre-CIE positive $\delta^{44/40}\text{Ca}$ shifts coincide with decreased test diameters of *R. cushmani* and correlate with decreases in the osmium isotope composition (Os_i) of seawater widely attributed to massive LIP inputs^{34–36}. Considered together, these observations reveal OAE2 as a geologic OA event. A return to lower $\delta^{44/40}\text{Ca}$ values during the main phase of OAE2 provides evidence for surface ocean alkalization in the aftermath of a biocalcification crisis, which in turn suggests that the Plenus Cold Event³⁷ could reflect a resulting period of transient CO₂ drawdown. Results from this study highlight the dynamic interplay between atmospheric CO₂ perturbations and biocalcification feedbacks, and further have implications for implementing ocean alkalinity enhancement as an anthropogenic climate change intervention strategy.

Results and discussion

Within the LCI of the Bottaccione section at Gubbio, bulk carbonate ($n = 31$) $\delta^{44/40}\text{Ca}$ values range from -1.56‰ to -1.45‰ and generally increase up-section through the LCI to the Last Occurrence (LO) of *R. cushmani* (Fig. 1); directly above this level, a sharp decrease in carbonate content prohibits further $\delta^{44/40}\text{Ca}$ analysis. The $\delta^{44/40}\text{Ca}$ values of coeval *R. cushmani* specimens ($n = 18$) start around -1.60‰ , concomitantly increase through the LCI to -1.41‰ , and then decrease to -1.48‰ just below the LO of the taxon at 110.85 msl (Fig. 1). The maximum *R. cushmani* $\delta^{44/40}\text{Ca}$ value of -1.41‰ occurs at 110.72 msl. This pattern of change in $\delta^{44/40}\text{Ca}$ relative to the LO of *R. cushmani* is identical to that observed in the Portland core, Western Interior Basin (WIB)³⁰ (Supplementary Fig. 5).

Observed changes in $\delta^{44/40}\text{Ca}$ values for *R. cushmani* significantly correlate with the specimens' Foraminiferal Abnormality Index (FAI; $p = 0.004$, $R^2 = 0.50$), which is defined as the percentage of malformed and/or deformed specimens¹⁸, as well as their Feret diameters ($p = 0.006$, $R^2 = 0.45$), but do not correlate with changes in coiling direction ($p = 0.14$, $R^2 = 0.17$; Fig. 2). At

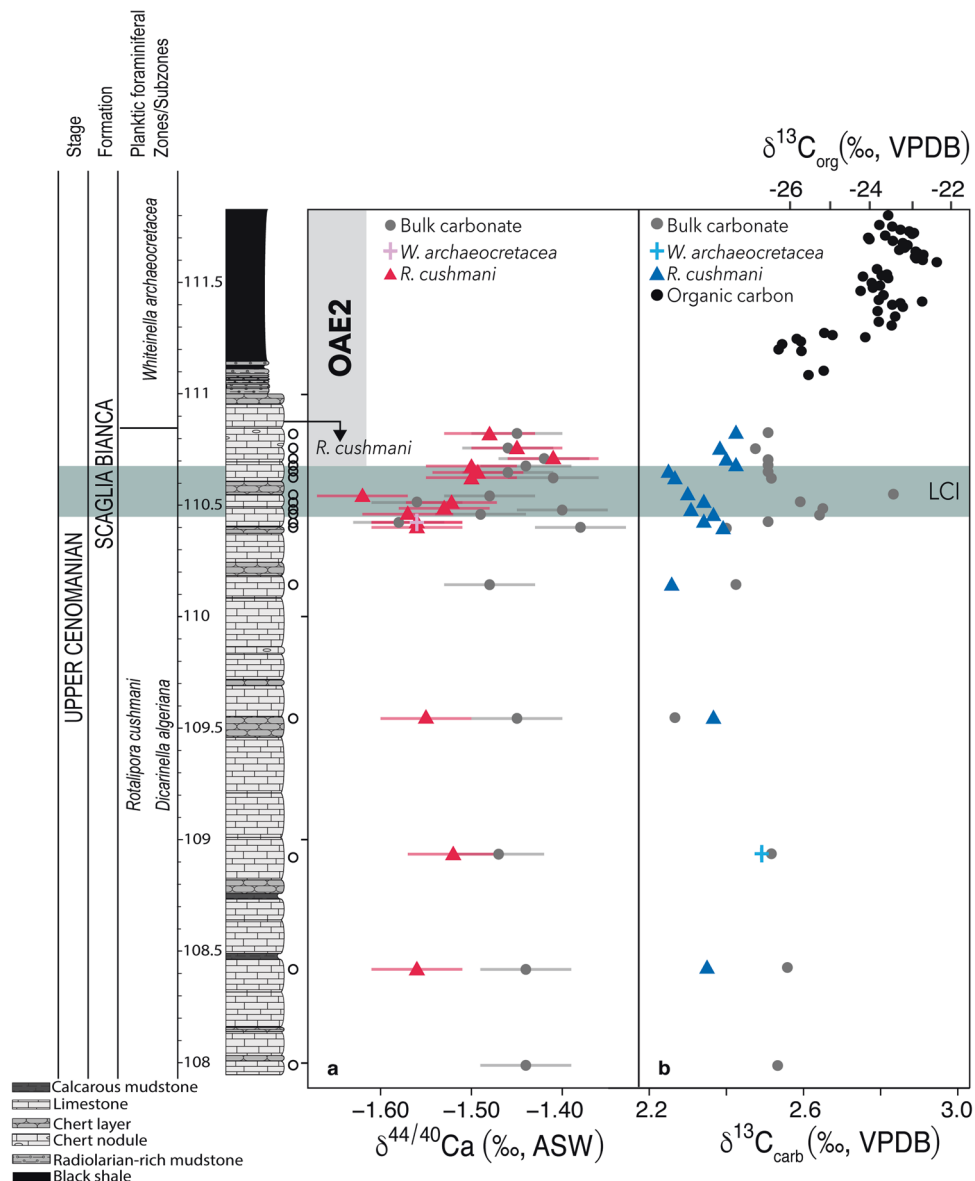


Fig. 1 Stratigraphic calcium and carbon isotope data from the Bottaccione section. Relative to stratigraphy of the Bottaccione section, **a** calcium isotope values ($\delta^{44/40}\text{Ca}$) of planktic foraminifera *Rotalipora cushmani* (red triangles), *Whiteinella archaeocretacea* (pink cross), and bulk carbonate (gray circles) where the error bars correspond to the analytical external reproducibility of ± 0.05 ($2\sigma_{\text{SD}}$), and **b** carbon isotope values of carbonate ($\delta^{13}\text{C}_{\text{carb}}$), including planktic foraminifera *Rotalipora cushmani* (blue triangles), *Whiteinella archaeocretacea* (blue cross), and bulk carbonate (gray circles). Oceanic Anoxic Event 2 is denoted by the positive $\delta^{13}\text{C}_{\text{org}}$ excursion⁷³ just below the black shale interval, here expressed at the Bonarelli Level. The last occurrence of *R. cushmani* is denoted by the downward pointing arrow. The open circles next to the stratigraphic column represent sample locations. LCI lower critical interval, ASW Atlantic Seawater; VPDB Vienna Pee Dee Belemnite.

one stratigraphic interval (110.43 msl), measurements were made for *R. cushmani* and another planktic foraminifer, *Whiteinella archaeocretacea*. The $\delta^{44/40}\text{Ca}$ values are identical (Fig. 1). Bulk carbonate ($n = 32$) $\delta^{44/40}\text{Ca}$ values from the AA core, WIB, which has an expanded succession comprising the onset of OAE2 relative to the Portland core and the Bottaccione section, range from -1.58‰ to -1.40‰ , with the maximum value well preceding the level of bentonite A, corresponding to the LO of *R. cushmani* (Supplementary Fig. 4). The positive $\delta^{44/40}\text{Ca}$ excursion spans both calcareous mudstone and limestone beds. Near the end of OAE2 in the Western Interior, stable and relatively negative $\delta^{44/40}\text{Ca}$ values similarly persist across multiple lithologies. All results presented here closely mirror a previously generated $\delta^{44/40}\text{Ca}$ record from the WIB³⁰.

Bulk $\delta^{13}\text{C}_{\text{carb}}$ measurements agree with previously generated records for the Bottaccione section (see Supplementary Fig. 5) and the AA core. In addition, comparisons between bulk and foraminiferal $\delta^{44/40}\text{Ca}$, $\delta^{13}\text{C}_{\text{carb}}$, and $\delta^{18}\text{O}$ values at Gubbio show that bulk values are on average heavier for all systems (Fig. 3). These differences are most visible within the lower section of the LCI, where bulk carbonate measurements are -0.18‰ heavier than *R. cushmani* for $\delta^{44/40}\text{Ca}$, at most 0.64‰ heavier for $\delta^{13}\text{C}_{\text{carb}}$, and $\sim 1\text{‰}$ heavier for $\delta^{18}\text{O}$. All data can be found in Supplementary Data 1.

Controls on the $\delta^{44/40}\text{Ca}$ system over short timescales. This study is primarily focused on trends in $\delta^{44/40}\text{Ca}$ values within the LCI preceding OAE2 (Fig. 1). Whereas a previous study focused

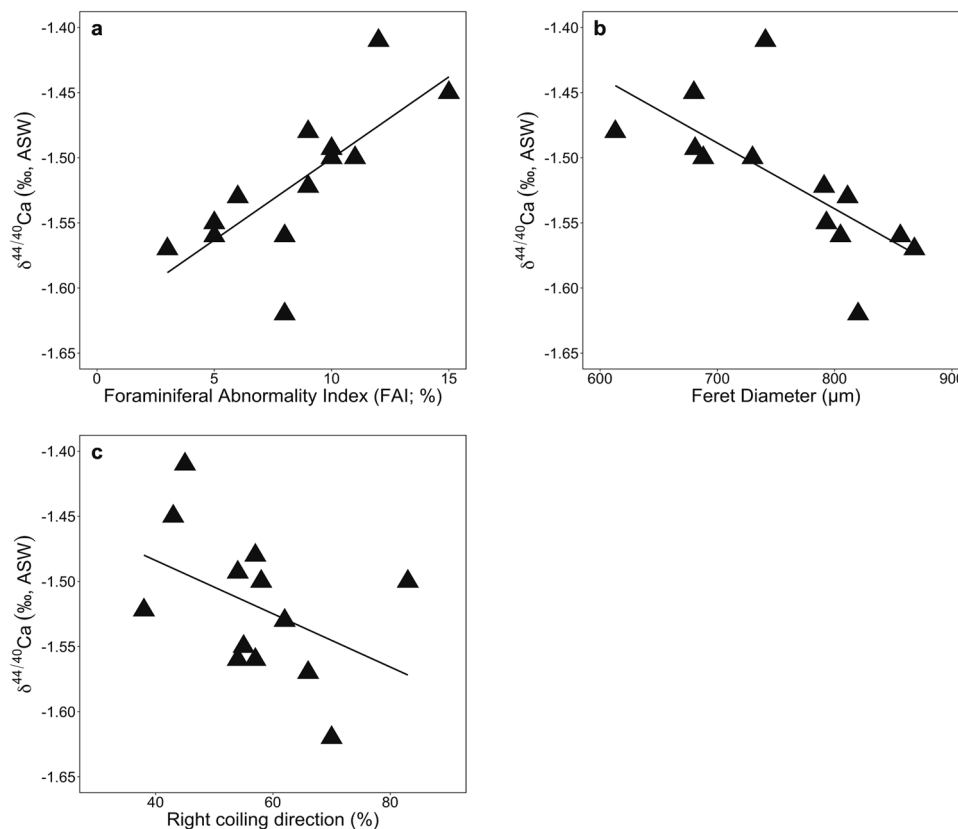


Fig. 2 Regression analyses of Bottaccione section $\delta^{44/40}\text{Ca}$ values and morphometric data. Planktic foraminifera *Rotalipora cushmani* $\delta^{44/40}\text{Ca}$ values across the lower critical interval (LCI) regressed against *R. cushmani* morphometric data published in Coccioni et al.¹⁸ shown in black triangles, including **a** Foraminiferal Abnormality Index or FAI, **b** Feret Diameter, and **c** Right coiling direction. Statistically significant relationships shown by black lines are observed between $\delta^{44/40}\text{Ca}$ and FAI ($p = 0.004$, $R^2 = 0.50$), as well as $\delta^{44/40}\text{Ca}$ and Feret Diameter ($p = 0.006$, $R^2 = 0.45$); however, the weak negative relationship between $\delta^{44/40}\text{Ca}$ and right coiled specimens is not significant ($p = 0.14$, $R^2 = 0.11$). ASW Atlantic Seawater.

on the long-term decrease in $\delta^{44/40}\text{Ca}$ values after OAE2 began³⁸, the LCI spans a timescale of only ~60 kyr preceding the positive shift in $\delta^{13}\text{C}$. Given the large inventory of Ca in seawater (~22 mmol/kg for Cretaceous seawater³⁹), combined with the element's long residence time ($\tau \approx 1$ Myr), input-output flux imbalances cannot substantially shift the Ca isotope composition of seawater over such short timescales^{31,40}. Rather, only two mechanisms can produce the observed trends, either addition of secondary Ca derived from seawater or changes in $\Delta_{\text{CaCO}_3-\text{H}_2\text{O}}$ during primary carbonate formation. We consider these hypotheses below.

Addition of secondary Ca. Due to slow reaction rates, little to no fractionation occurs when primary calcite recrystallizes and/or authigenic carbonate precipitates^{41,42}. If these diagenetic reactions are pervasive and occur under open system (fluid-buffered) conditions, then secondary incorporation of seawater Ca could elevate $\delta^{44/40}\text{Ca}$ values, thereby simulating effects from reduced precipitation rates⁴³. Conversely, if diagenesis is minimal or occurs under closed system conditions (sediment-buffered), then primary signals can be preserved⁴³.

Multiple observations show that the sediment piles at both sites experienced minimal fluid interactions. Modern diagenetic studies indicate low sediment-water interactions in depositional environments typifying the Bottaccione section (pelagic⁴⁴) and the AA core (hemipelagic⁴⁵)^{41,43}. Accordingly, bulk carbonates from both sites have low $\delta^{44/40}\text{Ca}$ values compared to carbonates altered under fluid-buffered conditions⁴⁶. The positive $\delta^{44/40}\text{Ca}$ excursions at the Bottaccione section underlay the organic-rich

Bonarelli Level. Organic matter (OM) respiration could have caused carbonate dissolution, thereby increasing fluid flow, resulting in authigenic carbonate precipitation⁴². Such a mechanism is expected to lower bulk $\delta^{13}\text{C}$ values, but in the LCI, bulk $\delta^{13}\text{C}$ values negligibly vary while $\delta^{44/40}\text{Ca}$ values clearly increase. Therefore, we find no evidence supporting a fluid-buffered diagenetic regime at our study sites.

Our study is the first to analyze foraminiferal and bulk $\delta^{44/40}\text{Ca}$ values from one location. The foraminiferal samples from the Bottaccione section show textural evidence for recrystallization and possible calcite infilling (see Supplementary Fig. 6). However, their $\delta^{44/40}\text{Ca}$ values are toward the lower range for calcite⁴⁷, and the values are either the same or lower than those for corresponding bulk carbonate (Fig. 3). The mostly unique $\delta^{44/40}\text{Ca}$ values of bulk carbonate and foraminifera indicate that the archives were not geochemically homogenized and are therefore high-fidelity. Furthermore, as *R. cushmani* composes a minor fraction (0.1–4.3%) of the bulk carbonate⁴⁸, differences between the archives suggest the infilled calcite contains Ca internally derived from test chambers. Apparent convergence for a few samples could represent homogenization, but presumably under sediment-buffered conditions, as these samples display both low and high $\delta^{44/40}\text{Ca}$ values. As discussed below, it is equally, if not more probable that the pattern reflects primary signals.

Environmental control of $\Delta_{\text{CaCO}_3-\text{H}_2\text{O}}$. Absence of evidence for authigenesis and fluid-buffered early-diagenetic control points to a reduction in the magnitude of $\Delta_{\text{CaCO}_3-\text{H}_2\text{O}}$ as the most plausible hypothesis for identical positive $\delta^{44/40}\text{Ca}$ excursions observed in

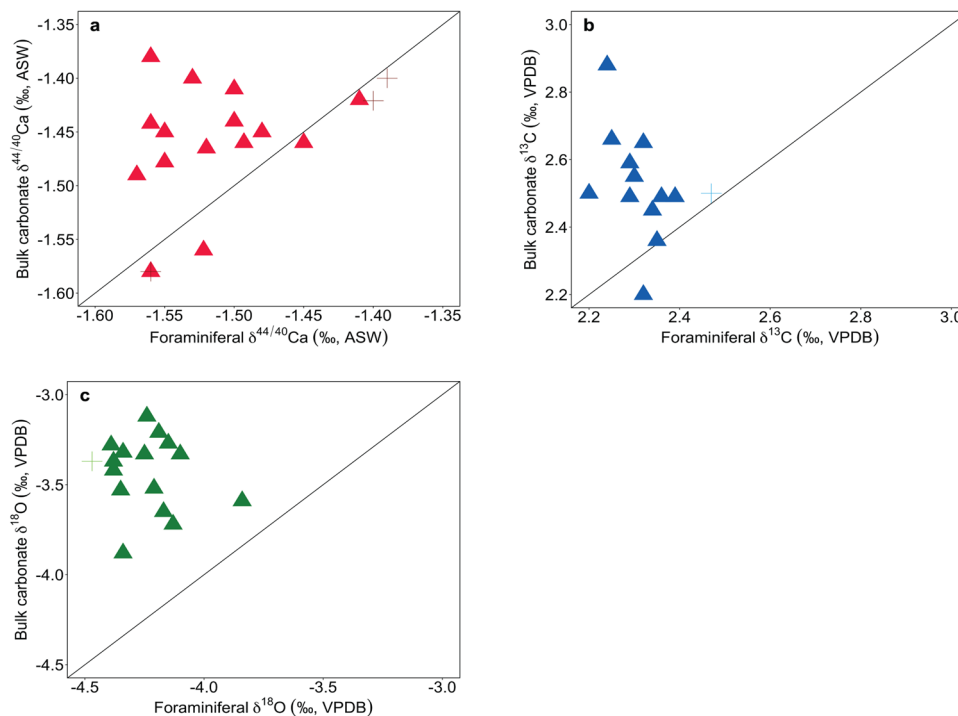


Fig. 3 Comparison of bulk carbonate and foraminiferal $\delta^{44/40}\text{Ca}$ values. Bottaccione section **a** foraminiferal $\delta^{44/40}\text{Ca}$ (*Rotalipora cushmani* in red triangles and *W. archaeocretacea* in pink crosses) against bulk carbonate $\delta^{44/40}\text{Ca}$ values, where the black line represents a 1:1 relationship between the different archives, **b** foraminiferal $\delta^{13}\text{C}$ (*Rotalipora cushmani* in blue triangles and *W. archaeocretacea* in a blue cross) against bulk carbonate $\delta^{13}\text{C}$ values, where the black line represents a 1:1 relationship between the different archives, and **c** foraminiferal $\delta^{18}\text{O}$ (*Rotalipora cushmani* in green triangles and *W. archaeocretacea* in a green cross) against bulk carbonate $\delta^{18}\text{O}$ values, where the black line represents a 1:1 relationship between the different archives. ASW Atlantic Seawater; VPDB Vienna Pee Dee Belemnite.

two different carbonate archives deposited in two globally separated locations. For both inorganic and biogenic carbonates, two primary environmental parameters influence $\Delta_{\text{CaCO}_3-\text{H}_2\text{O}}$: temperature and precipitation rate. In general, foraminiferal $\delta^{44/40}\text{Ca}$ values weakly relate to temperature^{49,50}, with the magnitude of $\Delta_{\text{CaCO}_3-\text{H}_2\text{O}}$ decreasing at higher temperatures²⁹ (Supplementary Fig. 1). While proxy temperature records with sufficient resolution do not exist from either the WIB or the Bottaccione section prior to OAE2, comparison of foraminiferal $\delta^{18}\text{O}$ values (a canonical paleo-thermometer) and $\delta^{44/40}\text{Ca}$ values at the Bottaccione section help constrain the influence of temperature on $\Delta_{\text{CaCO}_3-\text{H}_2\text{O}}$. No statistical relationship exists between the two proxies through the LCI ($p = 0.16$, $R^2 = 0.09$) (see Supplementary Fig. 7), and $\delta^{18}\text{O}$ values through the section only vary by 0.17‰, suggesting minimal temperature change during the LCI.

The data appear consistent with kinetic control of $\Delta_{\text{CaCO}_3-\text{H}_2\text{O}}$. In other words, carbonate chemistry dominates both inorganic²⁶ and foraminiferal calcite precipitation rates^{7,8}. Inorganic carbonate studies have demonstrated that decreased precipitation rates reduce the magnitude of $\Delta_{\text{CaCO}_3-\text{H}_2\text{O}}$ ^{26,41}, and some biogenic carbonates fractionate Ca isotopes similarly to inorganic calcite^{29,32,51,52} (Supplementary Fig. 1). Application of the stable Ca and Sr isotope ($\delta^{44/40}\text{Ca}$ - $\delta^{88/86}\text{Sr}$) multi-proxy to biogenic carbonates spanning OAE1a offers particularly strong evidence for precipitation rate control⁵¹. Across this paleoclimate event, $\delta^{44/40}\text{Ca}$ and $\delta^{88/86}\text{Sr}$ values correlate with a slope identical to the one predicted from kinetic theory and observed in inorganic calcite precipitation experiments⁵³, further confirming that most carbonates form kinetically²⁷.

Following from the above interpretation, the coincident foraminiferal and bulk records sampled in the Bottaccione

section present an opportunity to examine how, if at all, different organisms responded to carbonate chemistry stress. As noted above, *R. cushmani* composes a very small fraction of the pelagic bulk carbonate representing the LCI. Instead, nannofossils, particularly the coccolithophores *Biscutum constans* and *Zeugrhabdotus*²², dominate. While both foraminiferal and bulk carbonate archives show positive $\delta^{44/40}\text{Ca}$ excursions through the LCI, Fig. 3 shows that bulk carbonate has higher $\delta^{44/40}\text{Ca}$, $\delta^{13}\text{C}$, and $\delta^{18}\text{O}$ values than foraminifera. Previously studied Cretaceous sediments show that coccolith fractions have higher $\delta^{13}\text{C}$ and $\delta^{18}\text{O}$ values compared to deeper dwelling planktic foraminifera⁵⁴. As *R. cushmani* dwelled deeper in the thermocline⁵⁵, it follows that the higher bulk $\delta^{13}\text{C}$ and $\delta^{18}\text{O}$ values are weighted towards surface ocean calcifiers, such as coccoliths. Thus, we interpret the bulk $\delta^{44/40}\text{Ca}$ data as a record of surface ocean biocalcification stress, noting that the surface ocean signal may be muted, as bulk carbonate comprises both surface and thermocline dwelling species. Figure 1 may suggest that coccolithophores and other surface ocean calcifiers experienced biocalcification stress before *R. cushmani*, consistent with rapid surface OA and downward propagation of acidified waters. If our archives record species-specific responses, then the scatter observed in the Bottaccione bulk record may represent shifts in species abundances leading up to OAE2²² because the bulk records average numerous pelagic species. Changes in species abundance may also explain scatter in the AA record, particularly considering evidence for Tethyan and Boreal water-mass mixing, and resulting ecosystem shifts, before and during OAE2⁵⁶.

Relation to existing OAE2 records. The Ca isotope records presented in this study correlate with existing morphometric, ecological, and geochemical evidence consistent with OA and

carbon cycle perturbations leading up to OAE2. For example, nannofossil abundance data from the same section show that nannofossil extinctions began and persisted through the LCI^{20,22}. During the LCI (here defined to start ~60 kyr prior to the CIE) at the Bottaccione section, *R. cushmani* tests become smaller (show decreased Feret diameters), abnormal, and malformed, and their coiling directions change from right to left¹⁸. Above, we deduce that reduced precipitation rates were the principal driver of elevated $\delta^{44/40}\text{Ca}$ values through the LCI; therefore, we interpret the significant relationships between *R. cushmani* $\delta^{44/40}\text{Ca}$ values and two morphometric observations (FAI and Feret diameter) as consistent with OA-driven biocalcification stress. We note that foraminiferal morphometric proxies, particularly coiling direction¹⁸, have exhibited sensitivity to additional environmental parameters, such as salinity, temperature, oxygen content²⁵, and toxic metal loading²². While our analysis does not indicate that these stressors impacted the $\delta^{44/40}\text{Ca}$ records at the onset of the LCI, thallium isotope reconstructions provide evidence for global deoxygenation starting ~43 kyr prior to OAE2⁵⁷, which could have compounded biocalcification stress. Osmium isotope (Os_i) records for the WIB show that Os_i values declined prior to the onset of OAE2 and led the positive CIE by ~60 kyr³⁶. Using an integrated timescale to compare these Os_i records to our $\delta^{44/40}\text{Ca}$ records (see Supplementary Fig. 5), we show that the positive $\delta^{44/40}\text{Ca}$ excursions coincide with decreases in Os_i (Fig. 4). Furthermore, small decreases in the Os_i records ~300 kyr prior to OAE2 align with increased $\delta^{44/40}\text{Ca}$ values in the bulk carbonate records from the Portland core and the Bottaccione section. The overall correlation between $\delta^{44/40}\text{Ca}$ and Os_i is statistically significant ($p < 0.01$, Supplementary Fig. 10) but relatively weak ($R^2 = 0.38$), which we interpret as evidence for dynamic

biocalcification feedbacks on $\delta^{44/40}\text{Ca}$ as discussed below. The Os_i decrease most likely reflects a pulse of volcanism from the CLIP and/or High Arctic LIP^{35,36}. Previous studies of LIP eruptions across OAE2 suggest a slow rate of CO_2 addition¹⁶; however, our $\delta^{44/40}\text{Ca}$ records suggest this global CO_2 pulse occurred relatively rapidly, resulting in OA and biocalcification stress. The observation that elevated $\delta^{44/40}\text{Ca}$ values predate the CIE further indicates that calcification stress represents a principal response to increased CO_2 and that oceanic anoxia followed. Our study highlights that a reconceptualization of the onset of OAE2, to include the LCI, may be appropriate. At present, the initiation of OAE2 in the Gubbio section is defined by the positive shift in $\delta^{13}\text{C}_{\text{org}}$ values, whereas the Ca isotope proxy provides evidence that the volcanically-driven carbon cycle perturbation predates the CIE. If OAEs are truly global perturbations of the carbon cycle, then our results demonstrate that the perturbation began before the CIE recorded in $\delta^{13}\text{C}_{\text{org}}$. This view highlights a need to further focus on the pre-OAE2 interval, as defined by the LCI in the Bottaccione section.

Our multi-proxy correlations suggest that LIP volcanism caused a rapid influx of CO_2 leading up to OAE2, resulting in reduced biocalcification. Previous studies demonstrate that decreased biocalcification acts as a rapid negative feedback to OA³; however, the impact of biological compensation during continued CO_2 injection into the atmosphere-ocean system has received less attention. Just as chemical compensation (burn-down) increases ocean alkalinity via dissolution of carbonate sediments⁵⁸, biological compensation increases alkalinity in the surface ocean, thereby buffering the effects of OA³. If atmospheric CO_2 concentrations remain elevated after the initial biological compensation, then increased surface ocean alkalinity from

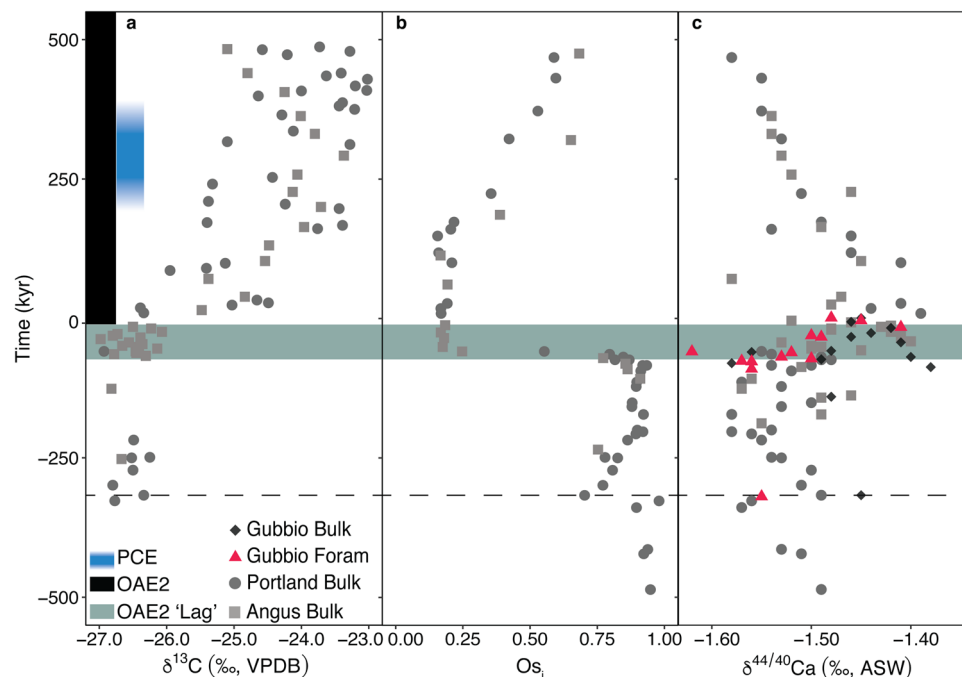


Fig. 4 A compilation of geochemical data preceding and across OAE2. Time series of **a** carbon isotope ($\delta^{13}\text{C}$) values from two sites, the AA core in gray squares (Joo and Sageman⁴⁵) and the Portland core in gray circles (Sageman et al.¹⁷), **b** osmium isotope (Os_i) from two sites, the AA core in gray squares (this study) and the Portland core in gray circles (Du Vivier et al.^{35,36}), and **c** calcium isotope values from three sites: the Gubbio Bottaccione section with foraminiferal measurements in red triangles and bulk carbonate in black diamonds (this study), the AA core in gray squares (this study), and the Portland core in gray circles (Du Vivier et al.³⁰). The gray shaded area marks the previously observed lag between the Os_i excursion indicating enhanced volcanism and the onset of the positive $\delta^{13}\text{C}$ excursion marking greater organic carbon burial³⁶, which corresponds to the lower critical interval. The dashed line marks a small decrease in Os_i and a small increase in $\delta^{44/40}\text{Ca}$ at roughly 300 kyr before OAE2 began. The timing of the Plenus Cold Event, shown with blue shading, follows from O'Connor et al.³⁷. PCE Plenus Cold Event, OAE2 Oceanic Anoxic Event 2, ASW Atlantic Seawater, VPDB Vienna Peedee Belemnite.

reduced biocalcification would enhance disequilibrium between the atmosphere and the surface ocean. The disequilibrium would cause CO₂ invasion to the surface ocean¹⁰, thereby creating a positive feedback loop of additional biocalcification stress and OA. The Portland core and AA $\delta^{44/40}\text{Ca}$ records indicate that OA persisted for another ~150 kyr after the start of OAE2. Thus, while toxic metal loading from LIP volcanism offers a leading hypothesis for declining nannofossil abundances at Gubbio²², an equally plausible mechanism may be biocalcification stress from episodic and rapid OA, exacerbated by biological compensation feedbacks and continued CO₂ input from LIP volcanism. Sustained suppressed biocalcification would have continued to increase alkalinity in the surface ocean causing additional atmospheric CO₂ drawdown. Recovery of $\delta^{44/40}\text{Ca}$ and Os_i values in the Portland core and AA cores is consistent with a geologically rapid biocalcification response to waning CO₂ inputs (Supplementary Fig. 12). Sedimentological records of carbonate weight percent provide evidence for alkalinity overshoots following other OA events, such as the Paleocene–Eocene Thermal Maximum⁵⁹. Interestingly, the shift to lower $\delta^{44/40}\text{Ca}$ values observed here coincides with an enigmatic global cooling event (Fig. 4), i.e., the Plenus Cold Event³⁷. Transient CO₂ drawdown due to biologically-mediated ocean alkalization provides a mechanism to explain why climate cooling occurred during an otherwise hothouse period.

Evidence for biocalcification feedbacks from LIP eruptions and shifts in air-sea CO₂ partitioning deduced from the Ca isotope study of OAE2 may have implications for implementing ocean alkalinity enhancement as a strategy for mitigating the anthropogenic climate crisis and OA. Our interpretations presented here support model findings that sustained and higher magnitude ocean alkalinity enhancement is needed to increase CO₂ drawdown while also mitigating OA⁶⁰. Observations of episodic OA during OAE2 suggest that if ocean alkalinity enhancement was lower in magnitude, and/or did not include addition of external alkalinity, then the OA mitigation co-benefits of the climate intervention strategy may be limited.

Understanding biological compensation during OAE2 further bears on the relationship between ballasting of OM and nannofossil carbonate production^{61,62}. Future studies centered on interactions between OA, reduced biocalcification, and the biological pump leading up to OAE2 may provide more insight into the cause(s) of widespread, albeit not global, oceanic anoxia and noncalcareous stratigraphic intervals. Given that the community composition and abundance of surface ocean plankton contribute to overall OM export⁶³, understanding how OA affects pelagic calcifiers may shed light on long-standing debates about enhanced productivity versus enhanced preservation as the cause of OAEs¹⁵. For example, if biocalcification stress on coccolithophores caused the efficiency of the biological pump to decline prior to OAE2, then thermal stratification, reduced deep sea ventilation, and enhanced OM preservation may represent the driver⁶⁴. On the other hand, if coccolith biocalcification stress opened a niche for diatom proliferation, as these siliceous taxa are largely generalists⁶⁵, then enhanced productivity offers a more probable explanation⁵⁷. Alternatively, it is simply possible that reduced carbonate production contributes to the appearance of enhanced OM productivity, as megafauna could have continued to support the biological pump.

Conclusion

Foraminiferal and bulk $\delta^{44/40}\text{Ca}$ records from the Bottaccione section in Gubbio Italy, as well as a bulk $\delta^{44/40}\text{Ca}$ isotope record from AA in the WIS, all show coincident elevated values ~60 kyr prior to OAE2. A statistically significant correlation between

$\delta^{44/40}\text{Ca}$ and Os_i, a well-established proxy for volcanism, indicates that the Ca isotope records reflect a reduction in the magnitude of $\Delta_{\text{CaCO}_3-\text{H}_2\text{O}}$ resulting from slower carbonate precipitation rates due to OA. At the Bottaccione section, these results occur in tandem with morphometric indicators of biocalcification stress on foraminifera, such as test dwarfing and malformation, which provide independent evidence for OA. The relationships between $\delta^{44/40}\text{Ca}$, $\delta^{13}\text{C}$, and $\delta^{18}\text{O}$ values of *R. cushmani* and bulk carbonate at the Bottaccione section further show that bulk carbonate records can capture the overall biocalcification response to OA, which could include major assemblage reorganization. While additional studies are needed to examine species-specific effects on $\Delta_{\text{CaCO}_3-\text{H}_2\text{O}}$, correlating the data to existing proxies for volcanic activity suggests that elevated atmospheric CO₂ levels from emplacement of the CLIP and/or High Arctic LIP decreased carbonate ion concentrations and $\Delta_{\text{CaCO}_3-\text{H}_2\text{O}}$ by extension. Given that both species-specific and bulk $\delta^{44/40}\text{Ca}$ values increase prior to OAE2, our data provide good evidence that elevated CO₂ and OA preceded the positive CIE, which points to a need to redefine the timing and cause(s) of the event. Elevated surface ocean alkalinity following reduced carbonate production would have facilitated additional atmospheric CO₂ drawdown, thereby sustaining biocalcification stress and creating a positive feedback loop for additional OA. The timing between elevated alkalinity and waning volcanic activity, as predicted by our records, coincides with a period of transient global cooling (i.e., the Plenus Cold Event). This study highlights OAE2 as the first geological analog for ocean alkalinity enhancement, which is a leading marine climate intervention strategy for mitigating anthropogenic climate change and ocean acidification.

Methods

Bulk carbonate sample collection and processing. The Scaglia Bianca Formation was sampled in outcrop at the Bottaccione section in Gubbio, Italy (43°21'56.04"N, 12°34'57.56"E; 597 m above sea level) following the stratigraphic scheme outlined in Coccioni and Premoli Silva (2015)⁶⁶. For each interval of interest, ~100 g of bulk rock was collected and sent to Northwestern University (NU). The Angus Aristocrat (AA) core, recovered from the north-central Colorado (40°14'32.97"N, 104°41'42.98"W; 1506 m above sea level), was sampled at NU. Prior to dissolution, bulk samples were crushed using a shatter box, or when weakly lithified, using a mortar and pestle, with a pure silica sand 'rinse' applied between samples to minimize potential for cross-contamination. Depending on approximate CaCO₃ wt%, ~27–100 mg of powder was reacted with 10 mL of 5% HNO₃, and the mixtures were placed on a rocker table for ~12 h to ensure complete dissolution. Samples were then filtered through 0.45 μm filters and stored in acid-washed LDPE bottles. Calcium concentrations were determined using a Thermo Scientific iCAP 6500 ICP-OES at NU.

Foraminiferal sample collection and processing. At the University of Urbino, ~100 g of bulk rock sampled from the Bottaccione section was treated with concentrated acetic acid following Lirer (2000)⁶⁷, sieved through a 63 μm mesh, and dried at 50 °C prior to disaggregation¹⁸. After washing the sediments through a 212 μm mesh sieve, *R. cushmani* tests were picked from the nannofossil-rich chalk. When possible, *W. archaeocretacea* tests were also picked. For each sampling interval, 15–25 specimens of *R. cushmani* and available *W. archaeocretacea* were picked from this size fraction, measured for their morphometric Feret diameter, and sent to NU. In the Radiogenic Isotope Geochemistry Laboratory at NU, seven *R. cushmani* and/or *W. archaeocretacea* were subsampled, lightly crushed, and homogenized prior to cleaning with MilliQ water following the procedure outlined in Barker et al.⁶⁸. While previous studies indicate that cleaning procedures produce no discernable effects for Ca isotope measurements³², the samples were nonetheless washed with MilliQ water to remove any contaminants from the disaggregation process. After cleaning, samples were dissolved in 5% HNO₃ and stored in acid-cleaned LDPE bottles. Calcium concentrations were determined from diluted stock solutions using a Thermo iCapQ quadrupole ICP-MS in the Quantitative Bio-element Imaging Center at NU.

Additional foraminifera from four sampling intervals were imaged using a Hitachi S3400N-II SEM at the Northwestern University Atomic and Nanoscale Characterization Experimental Center to confirm species identification, examine the texture of specimens, and identify potential authigenic precipitates, such as diagenetic crystallites⁶⁹ (Supplementary Fig. 6). Samples were mounted onto carbon-taped mounts, and multiple specimens from each sampling interval were imaged to assess inter-sample variability. The images confirm the species and also show calcite infilling of all foraminiferal shells across all sampling intervals; the implications of this infilling are addressed in the main text.

Calcium isotope ratios. Calcium isotope ratios ($^{44}\text{Ca}/^{40}\text{Ca}$) were measured at NU using a high-precision ^{43}Ca - ^{42}Ca double-spike technique⁷⁰ and a Thermo-Fisher Triton MC-TIMS equipped with 10^{11} Ω amplifier resistors. Data were collected periodically from June 2018 to October 2020. All procedures were conducted under clean room conditions and employed acid cleaned labware and ultrapure reagents. Blanks ($n = 7$) from labware, reagents, and foraminiferal cleaning procedures were quantified by isotope dilution and were found to be nearly 100 times lower than the sample size, which is negligible. Eight OSIL Atlantic Seawater (ASW) standards and two NIST SRM-915b standards were analyzed every 30 or fewer samples. Sample and standard volumes containing 50 μg of Ca for bulk carbonates and 25 μg of Ca for foraminiferal samples were spiked, and the mixtures were equilibrated on a hotplate at 60 °C for 12 h before drying down at 90 °C overnight. ASW standards and bulk carbonate samples were re-dissolved in 500 μL of 1.55 N HCl, and the solutions were passed through Teflon columns packed with Bio-Rad AG MP-50 cation exchange resin to separate Ca from K and other matrix elements. After drying down the purified fractions at 90 °C, OM was oxidized by adding two drops of 35% H_2O_2 , and Ca was converted to nitrate form by adding two drops of concentrated 16 N HNO_3 . The solutions were dried and re-dissolved in 5 μL of 3 N HNO_3 . For 915b, aliquots containing 50 μg of Ca were processed without column chemistry, and then two drops of 35% H_2O_2 were added, followed by two drops of concentrated 16 N HNO_3 . Foraminiferal samples were not processed through column chemistry due to their lower [Ca]. For all samples and standards, ~10–16 μg of Ca was loaded onto Ta filament assemblies. The double-spike was frequently recalibrated using the ASW data for each session⁷⁰. All results are reported in δ -notation relative to ASW, where $\delta^{44/40}\text{Ca}_{\text{amp}}(\%) = [(^{44}\text{Ca}/^{40}\text{Ca})_{\text{amp}} / (^{44}\text{Ca}/^{40}\text{Ca})_{\text{ASW}} - 1] \times 1000$.

During the period of study, repeated measurements of ASW and 915b yielded $\delta^{44/40}\text{Ca} = -0.002 \pm 0.039\%$ ($2\sigma_{\text{SD}}$, $n = 80$) and $\delta^{44/40}\text{Ca} = -1.147 \pm 0.055\%$ ($2\sigma_{\text{SD}}$, $n = 24$). AA data collection began in June 2018, whereas Gubbio data collection began in May 2019; however, it is worth noting that no significant differences exist between standard values measured during the data collection periods. Since implementation of the Lehn et al.⁷⁰ method, measurements of ASW and 915b have yielded $\delta^{44/40}\text{Ca} = 0.000 \pm 0.044\%$ ($2\sigma_{\text{SD}}$, $n = 706$) and $-1.136 \pm 0.049\%$ ($2\sigma_{\text{SD}}$, $n = 276$). Long-term data for the lab point to an external reproducibility of $\pm 0.05\%$, which is the uncertainty assigned to samples analyzed in the present study. Replicates, or reanalysis of the same dissolved sample were measured ($n = 9$). One duplicate sample, as well as analyses of altogether different samples taken from the same stratigraphic interval, were also analyzed. The difference between original measurements and replicates/duplicates is better than $\pm 0.05\%$.

Carbon and oxygen isotope analyses. Carbon and oxygen isotope ratios ($^{13}\text{C}/^{12}\text{C}$ and $^{18}\text{O}/^{16}\text{O}$) were measured at NU using a Thermo Scientific Delta V-Plus Isotope Ratio Mass Spectrometer (IRMS) equipped with a Gas Bench II, with a PAL autosampler. Approximately 200 μg of bulk sediment was measured into 12 mL glass Exetainers[®], which were then purged with UHP He gas for 10 mins prior to acidification with 200 μL of 103% H_3PO_4 , calibrated to a density of 1.92 g/cm^3 . The acidified samples were left to dissolve at 30 °C in an incubation block, for twelve hours. To optimize the isotope analyses for small samples (i.e., foraminifera), the above method was modified to maximize precision for masses ≤ 40 μg . Five foraminiferal samples were weighed into Sn capsules and subsequently placed into glass Exetainers[®]. These samples were also purged for 10 min with UHP He gas and placed in a thermostated temperature block for at least 30 min at 90 °C to ensure complete dissolution of the Sn capsule. Standards were analyzed at various size series to bracket the sample masses and to assess the linearity of corrections needed for sample $\delta^{13}\text{C}$ and $\delta^{18}\text{O}$ values. The resulting CO_2 from each sample was measured on the IRMS, following a variable mass standard series of NU in-house Carrara Lago marble standard (CLMS) ($\delta^{13}\text{C} = +2.31 \pm 0.05\%$, $\delta^{18}\text{O} = -3.70 \pm 0.10\%$), one NBS18 carbonate standard ($\delta^{13}\text{C} = -5.01 \pm 0.05\%$, $\delta^{18}\text{O} = -23.01 \pm 0.05\%$), and a blank. Approximately 200 μg of CLMS and NBS18, along with one blank, were repeatedly analyzed every ten samples and at the end of runs to assay instrumental drift. Carbon and oxygen isotope values are reported relative to the Vienna Pee Dee Belemnite standard ascertained by repeated analyses of NBS19 ($\delta^{13}\text{C} = +1.95\%$, $\delta^{18}\text{O} = -2.20\%$). For both $\delta^{13}\text{C}$ and $\delta^{18}\text{O}$ values, foraminiferal and bulk samples yielded the same $2\sigma_{\text{SD}}$ of $\pm 0.10\%$.

Statistical analyses. For non-serially correlated data (Bottaccione Section $\delta^{44/40}\text{Ca}$ and $\delta^{18}\text{O}$ values, as well as morphometric data), regression analysis was utilized to examine covariance between variables. Perhaps due to the small sample size, a Cook's distance plot indicated that two of the geochemical points composing the $\delta^{44/40}\text{Ca}$ - $\delta^{18}\text{O}$ correlation have high influence on the data. Thus, in order to consider the influence of each point on the regression, two alternate models were built where the data points were sequentially removed from each model. The results of each of these models suggest that no individual point influences the significance or strength of the R^2 value produced by the original model with all data points included. Therefore, no justification exists for excluding the points from the linear regression. These data meet all other assumptions for application of a linear model. Morphometric data from Coccioni et al.¹⁸ were selected for regression analyses, as the high sample number ($n = 4140$) likely best represents the *R. cushmani* population at the Bottaccione Section. The morphometric correlations meet all assumptions for application of a linear model.

For the studied time-series ($\delta^{44/40}\text{Ca}$ and WIB Os_i values), data were compiled into one dataset for correlation. Given that the individual datasets represent varied sampling intervals, we used the R package Astrochron surrogateCor function⁷¹ to examine the relationship between the datasets. This tool linearly interpolates the lower density sample set and then correlates the interpolated sample set with the higher resolution record for comparison. Due to the non-normality of all datasets, we implemented the non-parametric Spearman's Rank Correlation⁷². To examine whether one $\delta^{44/40}\text{Ca}$ dataset (Bottaccione Section, AA, or the Portland core) significantly influenced the correlation, the statistical analysis was also conducted using only one of the $\delta^{44/40}\text{Ca}$ datasets and the Os_i data. No differences were observed, indicating that no one record holds leverage in the combined regression analysis.

Data availability

All data generated in this study are available online at Zenodo (DOI: 10.5281/zenodo.7343671), as well as PANGAEA, and in the attached supplementary data file. The data file includes previously generated foraminiferal abnormality measurements¹⁸ and Os_i values for the WIB^{35,36}.

Received: 11 February 2022; Accepted: 22 November 2022;
Published online: 13 December 2022

References

- Schiebel R. Planktic foraminiferal sedimentation and the marine calcite budget. *Glob. Biogeochem. Cycles* 2002, **16**: 3–1–3–21.
- Berelson, W. et al. Relating estimates of CaCO_3 production, export, and dissolution in the water column to measurements of CaCO_3 rain into sediment traps and dissolution on the sea floor: a revised global carbonate budget. *Glob. Biogeochem. Cycles*, **21**, n/a–n/a (2007).
- Boudreau, B. P., Middelburg, J. J. & Luo, Y. The role of calcification in carbonate compensation. *Nat. Geosci.* **11**, 894 (2018).
- Si, W. & Rosenthal, Y. Reduced continental weathering and marine calcification linked to late Neogene decline in atmospheric CO_2 . *Nat. Geosci.* **12**, 833–838 (2019).
- Kump, L. R., Bralower, T. J. & Ridgwell, A. Ocean acidification in deep time. *Oceanography* **22**, 94–107 (2009).
- Hönisch, B. et al. The geological record of ocean acidification. *Science* **335**, 1058–1063 (2012).
- Osborne, E. B., Thunell, R. C., Gruber, N., Feely, R. A. & Benitez-Nelson, C. R. Decadal variability in twentieth-century ocean acidification in the California Current Ecosystem. *Nat. Geosci.* **13**, 43–49 (2020).
- Fox, L., Stukins, S., Hill, T. & Miller, C. G. Quantifying the effect of anthropogenic climate change on calcifying plankton. *Sci. Rep.* **10**, 1–9 (2020).
- Masson-Delmotte V., et al. IPCC, 2021: Climate Change 2021: The Physical Science Basis. Contribution of Working Group I to the Sixth Assessment Report of the Intergovernmental Panel on Climate Change. (Cambridge University Press, 2021).
- Kheshgi, H. S. Sequestering atmospheric carbon dioxide by increasing ocean alkalinity. *Energy* **20**, 915–922 (1995).
- Lenton, A., Matear, R. J., Keller, D. P., Scott, V. & Vaughan, N. E. Assessing carbon dioxide removal through global and regional ocean alkalization under high and low emission pathways. *Earth Syst. Dyn.* **9**, 339–357 (2018).
- Renforth, P. & Henderson, G. Assessing ocean alkalinity for carbon sequestration. *Rev. Geophys.* **55**, 636–674 (2017).
- Bach, L. T., Gill, S. J., Rickaby, R. E., Gore, S. & Renforth, P. CO_2 removal with enhanced weathering and ocean alkalinity enhancement: Potential risks and co-benefits for marine pelagic ecosystems. *Front. Clim.* **1**, 7 (2019).
- Foster, G. L., Royer, D. L. & Lunt, D. J. Future climate forcing potentially without precedent in the last 420 million years. *Nat. Commun.* **8**, 1–8 (2017).
- Jenkyns, H. C. Geochemistry of oceanic anoxic events. *Geochem. Geophys. Geosyst.* **11**, n/a–n/a (2010).
- Clapham, M. E. & Renne, P. R. Flood Basalts and Mass Extinctions. *Annu. Rev. Earth Planet. Sci.* **47**, 275–303 (2019).
- Sageman, B. B., Meyers, S. R. & Arthur, M. A. Orbital time scale and new C-isotope record for Cenomanian-Turonian boundary stratotype. *Geology* **34**, 125–128 (2006).
- Coccioni, R., Sideri, M., Frontalini, F. & Montanari, A. The Rotalipora cushmani extinction at Gubbio (Italy): planktonic foraminiferal testimonial of the onset of the Caribbean large igneous province emplacement. *Geol. Soc. Am. Spec. Pap.* **524**, 79–96 (2016).
- Barclay, R. S., McElwain, J. C. & Sageman, B. B. Carbon sequestration activated by a volcanic CO_2 pulse during Ocean Anoxic Event 2. *Nat. Geosci.* **3**, 205–208 (2010).

20. Erba, E., Bottini, C., Faucher, G., Gambacorta, G. & Visentin, S. The response of calcareous nannoplankton to Oceanic Anoxic Events: the Italian pelagic record. *Soc. Paleontol. Ital.* **58**, 51–71 (2019).
21. Leckie, R. M., Bralower, T. J. & Cashman, R. Oceanic anoxic events and plankton evolution: Biotic response to tectonic forcing during the mid-Cretaceous. *Paleoceanography*, **17**: 13–1–13–29, (2002).
22. Erba, E. Calcareous nannofossils and Mesozoic oceanic anoxic events. *Mar. Micropaleontol.* **52**, 85–106 (2004).
23. Coccioni, R. & Luciani, V. Planktonic foraminifera and environmental changes across the Bonarelli Event (OAE2, latest Cenomanian) in its type area: A high-resolution study from the Tethyan reference Bottaccione section (Gubbio, central Italy). *J. Foraminif. Res.* **34**, 109–129 (2004).
24. Coccioni, R., Erba, E. & Premoli-Silva, I. Barremian–Aptian calcareous plankton biostratigraphy from the Gorgo Cerbara section (Marche, central Italy) and implications for plankton evolution. *Cretac. Res.* **13**, 517–537 (1992).
25. Desmares, D. et al. A new proxy for Cretaceous paleoceanographic and paleoclimatic reconstructions: Coiling direction changes in the planktonic foraminifera *Muricohedbergella delrioensis*. *Palaeogeogr. Palaeoclimatol. Palaeoecol.* **445**, 8–17 (2016).
26. Tang, J., Dietzel, M., Böhm, F., Köhler, S. J. & Eisenhauer, A. Sr²⁺/Ca²⁺ and ⁴⁴Ca/⁴⁰Ca fractionation during inorganic calcite formation: II. Ca isotopes. *Geochim. Cosmochim. Acta* **72**, 3733–3745 (2008).
27. DePaolo, D. J. Surface kinetic model for isotopic and trace element fractionation during precipitation of calcite from aqueous solutions. *Geochim. Cosmochim. Acta* **75**, 1039–1056 (2011).
28. Nielsen, L. C., DePaolo, D. J. & De Yoreo, J. J. Self-consistent ion-by-ion growth model for kinetic isotopic fractionation during calcite precipitation. *Geochim. Cosmochim. Acta* **86**, 166–181 (2012).
29. Gussone, N. et al. Model for kinetic effects on calcium isotope fractionation (^{δ⁴⁴Ca}) in inorganic aragonite and cultured planktonic foraminifera. *Geochim. Cosmochim. Acta* **67**, 1375–1382 (2003).
30. Du Vivier, A. D. C. et al. Ca isotope stratigraphy across the Cenomanian–Turonian OAE 2: Links between volcanism, seawater geochemistry, and the carbonate fractionation factor. *Earth Planet. Sci. Lett.* **416**, 121–131 (2015).
31. Linzmeier, B. J. et al. Calcium isotope evidence for environmental variability before and across the Cretaceous–Paleogene mass extinction. *Geology* **48**, 34–38 (2020).
32. Kitch, G. D. et al. Calcium isotope composition of Morozovella over the late Paleocene–early Eocene. *Geology* **49**, 723–727 (2021).
33. Wang, J., Jacobson, A. D., Sageman, B. B. & Hurtgen, M. T. Stable Ca and Sr isotopes support volcanically triggered biocalcification crisis during Oceanic Anoxic Event 1a. *Geology* **49**, 515–519 (2021).
34. Turgeon, S. C. & Creaser, R. A. Cretaceous oceanic anoxic event 2 triggered by a massive magmatic episode. *Nature* **454**, 323 (2008).
35. Du Vivier, A. D. et al. Marine 187Os/188Os isotope stratigraphy reveals the interaction of volcanism and ocean circulation during Oceanic Anoxic Event 2. *Earth Planet. Sci. Lett.* **389**, 23–33 (2014).
36. Jones, M. M. et al. Regional chronostratigraphic synthesis of the Cenomanian–Turonian Oceanic Anoxic Event 2 (OAE2) interval, Western Interior Basin (USA): New Re–Os chemostratigraphy and 40Ar/39Ar geochronology. *Bulletin* **133**, 1090–1104 (2021).
37. O’Connor, L. K. et al. A re-evaluation of the Plenian Cold Event, and the links between CO₂, temperature, and seawater chemistry during OAE 2. *Paleoceanogr. Palaeoclimatol.* **35**, e2019PA003631 (2020).
38. Blättler, C. L., Jenkyns, H. C., Reynard, L. M. & Henderson, G. M. Significant increases in global weathering during Oceanic Anoxic Events 1a and 2 indicated by calcium isotopes. *Earth Planet. Sci. Lett.* **309**, 77–88 (2011).
39. Horita, J., Zimmermann, H. & Holland, H. D. Chemical evolution of seawater during the Phanerozoic: implications from the record of marine evaporites. *Geochim. Cosmochim. Acta* **66**, 3733–3756 (2002).
40. Komar, N. & Zeebe, R. Calcium and calcium isotope changes during carbon cycle perturbations at the end-Permian. *Paleoceanography* **31**, 115–130 (2016).
41. Fantle, M. S. & DePaolo, D. J. Ca isotopes in carbonate sediment and pore fluid from ODP Site 807A: The Ca₂+(aq)–calcite equilibrium fractionation factor and calcite recrystallization rates in Pleistocene sediments. *Geochim. Cosmochim. Acta* **71**, 2524–2546 (2007).
42. Fantle, M. S. & Ridgwell, A. Towards an understanding of the Ca isotopic signal related to ocean acidification and alkalinity overshoots in the rock record. *Chem. Geol.* **547**, 119672 (2020).
43. Higgins, J. et al. Mineralogy, early marine diagenesis, and the chemistry of shallow-water carbonate sediments. *Geochim. Cosmochim. Acta* **220**, 512–534 (2018).
44. Frontalini, F. et al. The Eocene Thermal Maximum 3: reading the environmental perturbations at Gubbio (Italy). *Stratigraphic Rec. Gubbio* **52A**, 161–326 (2016).
45. Joo, Y. J. & Sageman, B. B. Cenomanian to Campanian carbon isotope chemostratigraphy from the Western Interior Basin, USA. *J. Sediment. Res.* **84**, 529–542 (2014).
46. Ahm, A.-S. C. et al. An early diagenetic deglacial origin for basal Ediacaran “cap dolostones”. *Earth Planet. Sci. Lett.* **506**, 292–307 (2019).
47. Blättler, C. L., Henderson, G. M. & Jenkyns, H. C. Explaining the Phanerozoic Ca isotope history of seawater. *Geology* **40**, 843–846 (2012).
48. Coccioni, R. & Luciani, V. Planktonic foraminifera across the Bonarelli Event (OAE2, latest Cenomanian): the Italian record. *Palaeogeogr. Palaeoclimatol. Palaeoecol.* **224**, 167–185 (2005).
49. Sime, N. G., Christina, L. & Galy, A. Negligible temperature dependence of calcium isotope fractionation in 12 species of planktonic foraminifera. *Earth Planet. Sci. Lett.* **232**, 51–66 (2005).
50. Griffith, E. M., Paytan, A., Kozdon, R., Eisenhauer, A. & Ravelo, A. C. Influences on the fractionation of calcium isotopes in planktonic foraminifera. *Earth Planet. Sci. Lett.* **268**, 124–136 (2008).
51. Wang, J., Jacobson, A. D., Sageman, B. B. & Hurtgen, M. T. Stable Ca and Sr isotopes support volcanically triggered biocalcification crisis during Oceanic Anoxic Event 1. *Geology* **49**, 515–519 (2021).
52. Mejía, L. M. et al. Controls over ^{δ⁴⁴Ca} and Sr/Ca variations in coccoliths: new perspectives from laboratory cultures and cellular models. *Earth Planet. Sci. Lett.* **481**, 48–60 (2018).
53. Böhm, F. et al. Strontium isotope fractionation of planktic foraminifera and inorganic calcite. *Geochim. Cosmochim. Acta* **93**, 300–314 (2012).
54. Ando, A., Huber, B. T. & MacLeod, K. G. Depth-habitat reorganization of planktonic foraminifera across the Albian/Cenomanian boundary. *Paleobiology* **36**, 357–373 (2010).
55. Corfield, R., Hall, M. & Brasier, M. Stable isotope evidence for foraminiferal habitats during the during of the Cenomanian/Turonian ocean anoxic event. *Geology* **18**, 175–178 (1990).
56. Eldrett, J. S., Dodsworth, P., Bergman, S. C., Wright, M. & Minisini, D. Water-mass evolution in the Cretaceous western interior seaway of North America and equatorial Atlantic. *Climate* **13**, 855–878 (2017).
57. Ostrander, C. M., Owens, J. D. & Nielsen, S. G. Constraining the rate of oceanic deoxygenation leading up to a Cretaceous Oceanic Anoxic Event (OAE-2: ~94 Ma). *Sci. Adv.* **3**, e1701020 (2017).
58. Zeebe, R. E. History of seawater carbonate chemistry, atmospheric CO₂, and ocean acidification. *Annu. Rev. Earth Planet. Sci.* **40**, 141–165 (2012).
59. Penman, D. E. et al. An abyssal carbonate compensation depth overshoot in the aftermath of the Palaeocene–Eocene Thermal Maximum. *Nat. Geosci.* **9**, 575 (2016).
60. Ilyina, T., Wolf-Gladrow, D., Munhoven, G. & Heinze, C. Assessing the potential of calcium-based artificial ocean alkalization to mitigate rising atmospheric CO₂ and ocean acidification. *Geophys. Res. Lett.* **40**, 5909–5914 (2013).
61. Klaas, C., Archer, D. E. Association of sinking organic matter with various types of mineral ballast in the deep sea: Implications for the rain ratio. *Glob. Biogeochem. Cycles* **16**, 63–61–63–14 (2002).
62. Barker, S., Higgins, J. A. & Elderfield, H. The future of the carbon cycle: review, calcification response, ballast and feedback on atmospheric CO₂. *Philos. Trans. R. Soc. Lond. Ser. A* **361**, 1977–1999 (2003).
63. Weber, T. S. & Deutsch, C. Ocean nutrient ratios governed by plankton biogeography. *Nature* **467**, 550–554 (2010).
64. Arthur, M., Schlanger, S. T. & Jenkyns, H. The Cenomanian–Turonian Oceanic Anoxic Event, II. Palaeoceanographic controls on organic-matter production and preservation. *Geol. Soc. Lond. Spec. Publ.* **26**, 401–420 (1987).
65. Julius, M. L. & Theriot, E. C. The diatoms: a primer. *Appl. Environ. Earth Sci.* **2**, 8–22 (2010).
66. Coccioni, R. & Premoli-Silva, I. Revised Upper Albian–Maastrichtian planktonic foraminiferal biostratigraphy and magneto-stratigraphy of the classical Tethyan Gubbio section (Italy). *Newsl. Stratigr.* **48**, 47–90 (2015).
67. Lirer, F. A new technique for retrieving calcareous microfossils from lithified lime deposits. *Micropaleontology* **46**, 365–369 (2000).
68. Barker, S., Greaves, M. & Elderfield, H. A study of cleaning procedures used for foraminiferal Mg/Ca paleothermometry. *Geochim. Geophys. Geosyst.* **4**, n/a–n/a (2003).
69. Kozdon, R. et al. In situ ^{δ¹⁸O} and Mg/Ca analyses of diagenetic and planktic foraminiferal calcite preserved in a deep-sea record of the Paleocene–Eocene thermal maximum. *Paleoceanography* **28**, 517–528 (2013).
70. Lehn, G. O., Jacobson, A. D. & Holmden, C. Precise analysis of Ca isotope ratios (^{δ⁴⁴Ca}) using an optimized ⁴³Ca–⁴²Ca double-spike MC-TIMS method. *Int. J. Mass Spectrom.* **351**, 69–75 (2013).
71. Meyers S. Astrochron: An R package for astrochronology. Available at cran.rproject.org/web/packages/astrochron/index.html 2014.
72. Hauke, J., Kossowski, T. Comparison of values of Pearson’s and Spearman’s correlation coefficient on the same sets of data. 2011.
73. Tsikos, H. et al. Carbon-isotope stratigraphy recorded by the Cenomanian–Turonian Oceanic Anoxic Event: correlation and implications based on three key localities. *J. Geol. Soc.* **161**, 711–719 (2004).

Acknowledgements

We thank NU IRMS Laboratory Manager Andrew Masterson who assisted with stable isotope data collection. We also thank Tirzah Abbot for assisting with SEM training and imaging. Members of the Jacobson Laboratory Group provided many useful discussions. In addition, we thank Encana Inc. for donating the Aristocrat Angus core to Northwestern University and the USGS Core Research Center in Denver, CO for facilitating transfer of core material. We also thank two anonymous reviewers for their contributions in improving the manuscript. This work was supported by a NSF-GRFP (Grant No. DGE-1842165) awarded to GDK, as well as a David and Lucile Packard Foundation Fellowship (2007-31757) and a NSF grant (NSF-EAR 0723151) awarded to ADJ. The National Oceanic and Atmospheric Administration Ocean Acidification Program and the Illinois Indiana Sea Grant supported GDK during revision of this manuscript.

Author contributions

G.D.K. (corresponding author; gabby.kitch@noaa.gov): Contributed to designing the work, acquiring, analyzing and interpreting data, generating figures, and drafting and revising the manuscript. Corresponding author. A.D.J.: Contributed to designing the work, interpreting data, and drafting and revising the paper. B.B.S.: Contributed to designing the work, interpreting data, and drafting and revising the paper. R.C.: Contributed to designing the work, interpreting data, and revising the paper. T.-C.S.: Contributed to acquiring data and revising the paper. M.E.A.: Contributed to acquiring and analyzing data, as well as revising the paper. M.T.H.: Contributed to interpreting data and revising the paper. Key phrases: ocean acidification, geological proxies, calcium isotope record, Ocean Anoxic Event 2, ocean carbon dioxide removal, ocean alkalinity enhancement, Plenus Cold Event.

Competing interests

The authors declare no competing interests.

Additional information

Supplementary information The online version contains supplementary material available at <https://doi.org/10.1038/s43247-022-00641-0>.

Correspondence and requests for materials should be addressed to Gabriella D. Kitch.

Peer review information *Communications Earth & Environment* thanks the anonymous reviewers for their contribution to the peer review of this work. Primary Handling Editors: Joseph Aslin and Aliénor Lavergne. Peer reviewer reports are available.

Reprints and permission information is available at <http://www.nature.com/reprints>

Publisher's note Springer Nature remains neutral with regard to jurisdictional claims in published maps and institutional affiliations.



Open Access This article is licensed under a Creative Commons Attribution 4.0 International License, which permits use, sharing, adaptation, distribution and reproduction in any medium or format, as long as you give appropriate credit to the original author(s) and the source, provide a link to the Creative Commons license, and indicate if changes were made. The images or other third party material in this article are included in the article's Creative Commons license, unless indicated otherwise in a credit line to the material. If material is not included in the article's Creative Commons license and your intended use is not permitted by statutory regulation or exceeds the permitted use, you will need to obtain permission directly from the copyright holder. To view a copy of this license, visit <http://creativecommons.org/licenses/by/4.0/>.

This is a U.S. Government work and not under copyright protection in the US; foreign copyright protection may apply 2022